



# JGR Solid Earth

## RESEARCH ARTICLE

10.1029/2019JB018119

### Key Points:

- The modified centroid method is found most suitable for the DBMS estimation while the window sizes are 5 times of the target depth or more
- The shallow DBMS regions are highly correlated with the Ophiolite belts implying that the DBMS is not a good proxy for Curie depth
- The DBMS of 40 km in the Makran implies that the region is underlain by thick sediments and an old cold oceanic lithosphere

### Correspondence to:

A. R. Bansal,  
abhey.bansal@gmail.com

### Citation:

Kumar, R., Bansal, A. R., & Ghods, A. (2020). Estimation of depth to bottom of magnetic sources using spectral methods: Application on Iran's aeromagnetic data. *Journal of Geophysical Research: Solid Earth*, 125, e2019JB018119. <https://doi.org/10.1029/2019JB018119>

Received 29 MAY 2019

Accepted 22 FEB 2020

Accepted article online 26 FEB 2020

## Estimation of Depth to Bottom of Magnetic Sources Using Spectral Methods: Application on Iran's Aeromagnetic Data

Raj Kumar<sup>1,2</sup>, A. R. Bansal<sup>1</sup> , and Abdolreza Ghods<sup>3</sup>

<sup>1</sup>CSIR-National Geophysical Research Institute, Hyderabad, India, <sup>2</sup>Now at Shillong Geophysical Research Centre (IIG Mumbai), Shillong, India, <sup>3</sup>Department of Earth Sciences, Institute for Advanced Studies in Basic Sciences, Zanjan, Iran

**Abstract** The effect of window size while estimating the depth to bottom of magnetic sources (DBMS) is examined on the synthetic 2-D magnetic field data. The data are generated for 3-D fractal magnetization models assuming different combinations of depth to the top and bottom of magnetic sources. The depths are estimated assuming an uncorrelated and correlated random distribution of sources. The depths to the top estimated for fractal distribution of sources are found within 70% of the true values for all window sizes, whereas the values for the uncorrelated random distributions are far from the real depths. The DBMS for the correlated random distribution of sources are estimated within 70–80% of the true values for the window sizes of 5 times or more of the targeted depths. The modified centroid method is found to provide better estimations as compared to scaling-spectral peak modeling. The modified centroid method is applied to the aeromagnetic data of Iran to estimate the DBMS using a window size of  $200 \times 200 \text{ km}^2$ . The shallow DBMS between 12 and 20 km are obtained for the Quaternary Sabalan and Sahand volcanoes to the NW of Iran, the central and NE of central Iran, the central Zagros, NW of Tabas block, and the south of the Lut Block. The deepest DBMS of the order of 40 km is found in the Makran. The rest of Iranian Plateau is characterized by DBMS of 20 to 30 km. The shallow DBMS are found in correlation with the depth of the Ophiolites.

## 1. Introduction

The knowledge of temperature within the Earth is important to constrain the thermal structure and the rheological nature of the lithosphere. Bore-hole heat flow data can provide the most precise information about the geothermal structure but these measurements are very sparse and mostly limited to shallow depths. As an alternative, the depth to the bottom of magnetic sources (DBMS) has been conventionally used as a proxy for the Curie-point depth (Curie depth) and the heat flow in the region. The depth at which the magnetized materials lose their remnant magnetization due to the increasing of crustal temperature above Curie temperature is called Curie depth. The Curie temperature for magnetite, the most important ferrimagnetic mineral on the Earth, is about  $\sim 580^\circ\text{C}$ .

The different methods for estimation of the DBMS from aeromagnetic/magnetic data can be classified into two main classes, namely, those based on uncorrelated random (Bhattacharyya & Leu, 1975; Spector & Grant, 1970; Blakely, 1988; Okubo et al., 1985; Tanaka et al., 1999) and correlated random (Bansal et al., 2011, 2016; Bouligand et al., 2009; Chen et al., 2016; Dimri, 2005; Fedi et al., 1997; Kumar et al., 2018; Maus et al., 1997; Pilkington & Todoschuck, 1993; Ravat et al., 2007) spatial distribution of magnetic sources. The correlated random distribution of sources is also known as scaling distribution. All the above methods of DBMS estimation work in the frequency domain because convolution operators in the space domain become multiplication in this domain. In all the methods, the two-dimensional power spectrum of aeromagnetic data is estimated and then converted to 1-D radially averaged power spectrum. The majority of the authors have used the logarithm of the radial average power spectrum (e.g., Bansal et al., 2011, 2013; Blakely, 1988, 1995; Li et al., 2010, 2013; Okubo & Matsunaga, 1994; Ross et al., 2006; Tanaka et al., 1999) and some have used the radial average of the logarithm of power spectrum (e.g., Dolmaz et al., 2005; Maus & Dimri, 1995; Teknik & Ghods, 2017). The shape of the power spectrum in these two cases may differ with a change in estimated values up to 20% (Maus & Dimri, 1995). In the present study, we first take a radial average and then logarithm of the power spectra as this is the most used practice.

The DBMS corresponds to the base of the top magnetic layer of the crust. Therefore, large wavelength anomalies are required for the estimation of the DBMS from aeromagnetic data. The deep magnetized

bodies produce long wavelength and low amplitude anomalies whereas shallow magnetic sources relatively produce short wavelength and large-amplitude anomalies. In the spectral method, wavenumbers are used which are reciprocal to wavelengths. The depth of the deep magnetized bodies can be inferred from low wavenumbers part of the spectrum of aeromagnetic data (Bhattacharyya & Leu, 1975; Spector & Grant, 1970). To estimate the depth of the deep magnetic bodies, an optimum large window of magnetic anomalies containing the long wavelengths is required. Many studies used an arbitrary window size to estimate the DBMS, e.g.,  $60 \times 90$  (Okubo et al., 1985),  $90 \times 90$  (Dolmaz et al., 2005),  $1,000 \times 1,000$  (Maus et al., 1997), and  $320 \times 320$  km (Chiozzi et al., 2005). Blakely (1995) suggested a minimum window size of  $50 \times 50$  and  $160 \times 160$  km to resolve the Curie depth of 10 and 50 km, respectively. Ravat et al. (2007) recommend a window size  $>300$  to 500 km for the estimation of the deepest DBMS. Li et al. (2010) estimated the DBMS for three window sizes of  $68.9 \times 68.9$ ,  $99.2 \times 99.2$ , and  $144.5 \times 144.5$  km and found large differences in the estimated DBMS values. Recently, Li et al. (2017) presented the global reference model of the DBMS by taking the average of the DBMS obtained from three window sizes of  $98.8 \times 98.8$ ,  $195 \times 195$ , and  $296.4 \times 296.4$  km. Averaging of the DBMS found from different window sizes may be misleading. By increasing the window sizes, the magnetic data become nonstationary due to the inclusion of different geological entities (Bansal & Dimri, 1999). Therefore, it is always better to decide about the optimum window size before computing the DBMS. The synthetic data modeling is the best way to select optimum window size because we have full control over the true values of the top and bottom magnetic layer and comparison between the true and estimated depths become easy.

We carry out a systematic study to find the effects of different window sizes for estimation of the depth to the top of magnetic sources as well as the DBMS on a synthetic data set. We apply centroid and spectral peak modeling (SPM) methods for correlated (scaling/fractal) and uncorrelated distribution of sources. The suitable DBMS estimation method has been applied to the aeromagnetic data of Iran (<http://doi.org/10.5281/zenodo.3554861>) while using an appropriate window size. The success of the method to capture the undulations of Curie depth has been investigated in the light of available geological knowledge in the region.

## 2. Theory

Blakely (1995) presented a relation between power spectra of the magnetic field and magnetization in terms of depth to top and bottom of an anomalous body while assuming a constant vertical magnetization for the uncorrelated source distribution (Spector & Grant, 1970). The power spectra of the total magnetic anomaly can be written as

$$P(k_x, k_y, Z_t, Z_b) = 4\pi^2 C_m^2 \varphi_m(k_x, k_y) |\Theta_m|^2 |\Theta_f|^2 e^{-2|k|Z_t} \left(1 - e^{-|k|(Z_b - Z_t)}\right)^2, \quad (1)$$

where  $C_m$  is a proportionality constant;  $\varphi_m$  is the power spectrum of the magnetization;  $k_x$  and  $k_y$  are the wavenumbers in the  $x$  and  $y$  directions and their Euclidean norm,  $k = \sqrt{k_x^2 + k_y^2}$ , in  $2\pi/\text{km}$ ;  $\Theta_m$  and  $\Theta_f$  are the directional factors related to the magnetization and geomagnetic field, respectively;  $Z_t$  and  $Z_b$  are the depths to the top and bottom of the magnetic slab. In the case of the one-dimensional radial average power spectrum, terms  $\Theta_m$  and  $\Theta_f$  become constant. The magnetization term,  $\varphi_m$ , becomes constant for a random and uncorrelated distribution of sources.

From several bore-hole studies, it is found that magnetic sources are correlated in space and have a colored amplitude spectrum in the frequency domain (Pilkington & Todoeschuck, 1993, 1995; Maus & Dimri, 1994; Fedi et al., 1997). In case of fractal/scaling nature of source distribution, equation (1) subsequently can be written in terms of 1-D radially averaged power spectrum as (e.g., Bansal et al., 2011; Li et al., 2017)

$$P(k, Z_t, Z_b, \beta) = A_1 k^{-\beta} e^{-2|k|Z_t} \left(1 - e^{-|k|(Z_b - Z_t)}\right)^2, \quad (2)$$

where  $A_1$  is a constant and  $\beta$  is the scaling exponent related to lithology and heterogeneity of the subsurface (Bansal et al., 2010, 2011).

### 2.1. Centroid Method

The centroid method was originally proposed by Bhattacharyya and Leu (1975, 1977). The method involves the estimation of the top and centroid depth of the horizontally seated magnetic slab of

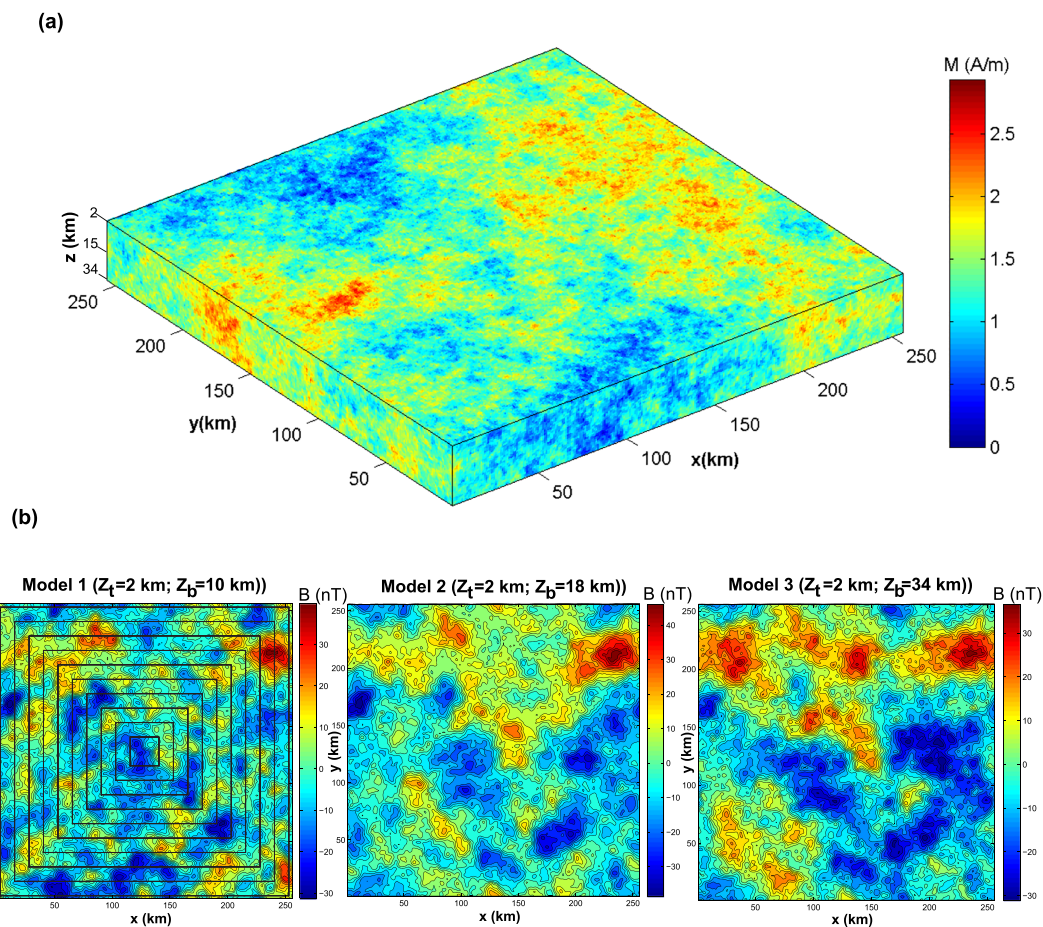


**Figure 1.** Synthetic 3-D fractal magnetization models (scaling exponent,  $\alpha = 3$ ) of different DBMS and their 2-D magnetic anomalies. (a) A 3-D fractal magnetization subspace of model 3. (b) Magnetic anomalies for model 1, model 2, and model 3 generated for constant depth to the top of 2 km and different bottom depth of 10, 18, and 34 km, respectively. Selected window sizes are shown in model 1 having midpoint as the center.

uniform magnetization from the radially averaged power spectrum of the magnetic data. Later, the method was modified for ensembles of sources with random magnetization (e.g., Okubo et al., 1985; Tanaka et al., 1999).

Moreover, for scaling source distribution, equation (2) can be simplified in terms of centroid depth ( $Z_0$ ) as

$$P(k, Z_t, Z_0, Z_b, \beta) = A_2 k^{-\beta} e^{-|k|Z_0} \left( e^{-|k|(Z_t - Z_0)} - e^{-|k|(Z_b - Z_0)} \right), \quad (3)$$

where  $A_2$  is constant. The centroid depth can be expressed in terms of depths to the top and bottom of the magnetic body as  $Z_b = 2Z_0 - Z_t$  (Okubo et al., 1985; Tanaka et al., 1999).

Equation (3) can be simplified in terms of the centroid depth at low wavenumbers of the radially averaged power spectra (e.g., Bansal et al., 2011),

$$\ln\left(\frac{P(k)}{k^2}\right) = A_3 - 2kZ_0 - \beta \ln(k), \quad (4)$$

where  $A_3$  is constant. The method is called a modified centroid method.

Considering random and uncorrelated source distribution ( $\beta = 0$ ), equation (4) can be converted to the centroid method (Tanaka et al., 1999),

**Table 1**

*Estimated Depth to Top for Three Sets of the Assumed Model Using Conventional (Centroid, Spectral Peak Modeling (SPM)) and Fractal Approach (Modified Centroid, Scaling-SPM) at Different Window Sizes*

Model	Assumed Top depth, $z_t$ (km)	Window size (km × km)	Calculated Top depth $z_t$ (km)			
			Conventional approach		Fractal approach	
			Centroid method	Spectral peak modeling (SPM)	Modified centroid method	Scaling-SPM
1	2	25 × 25	2.35	3.9	1.89	1.9
		50 × 50	2.44	6.5	1.64	2.8
		75 × 75	2.99	6.5	1.83	2.6
		100 × 100	3.12	6.5	1.94	3.5
		125 × 125	2.99	5.5	1.83	2.8
		150 × 150	4.55	6.5	2.21	3.1
		175 × 175	3.76	6.5	2.02	3.9
		200 × 200	4.06	7.0	2.01	4.0
		225 × 225	3.33	7.5	2.12	4.2
		250 × 250	3.9	7.5	1.98	4.4
2	2	25 × 25	2.53	3.0	1.53	1.6
		50 × 50	2.43	3.7	1.56	2.4
		75 × 75	2.89	4.6	1.73	3.5
		100 × 100	3.31	5.3	1.6	4.0
		125 × 125	3.4	5.6	1.86	3.5
		150 × 150	3.38	5.8	1.49	4
		175 × 175	3.3	5.6	1.53	4
		200 × 200	2.9	5.85	1.33	4
		225 × 225	2.74	6	1.47	4
		250 × 250	2.92	6.2	3.1	4.3
3	2	25 × 25	2.89	3.0	1.52	1.8
		50 × 50	3.07	3.5	1.53	2.3
		75 × 75	2.86	4.7	1.79	5
		100 × 100	2.89	5.2	1.64	5.5
		125 × 125	3.15	5	1.63	5.5
		150 × 150	3.21	5	1.81	6.5
		175 × 175	2.99	6	1.47	7
		200 × 200	2.82	6.5	1.83	7.5
		225 × 225	3.11	6.4	1.47	7.5
		250 × 250	3.37	6.5	1.9	8

$$\ln\left(\frac{P(k)}{k^2}\right) = A_3 - 2kZ_0. \quad (5)$$

For medium to high wavenumbers, equation (2) can be rewritten as (Bansal et al., 2011; Fedi et al., 1997; Maus & Dimri, 1995)

$$\ln\{P(k)\} = A_4 - 2|k| Z_t - \beta \ln(k), \quad (6)$$

where  $A_4$  is constant. For random and uncorrelated source distribution (Spector & Grant, 1970), equation (6) can be simplified as

$$\ln\{P(k)\} = A_4 - 2|k| Z_t. \quad (7)$$

## 2.2. Spectral Peak Modelling (SPM)

The spectral peak method (Blakely, 1995; Connard et al., 1983) is only efficient in the presence of a spectral peak in the Fourier spectra for an appropriate window size (Ravat et al., 2007). To overcome this limitation, Ravat et al. (2007) proposed forward modeling for iterative matching of the spectral peak by using a modified version of equation (2) and named it as SPM,

**Table 2**

*Estimated Depth to Bottom for Three Sets of Assumed Models Using Conventional (Centroid, Spectral Peak Modeling (SPM)) and Scaling Approach (Modified Centroid, Scaling-SPM) at Different Window Sizes*

Model	Assumed bottom depth, $z_b$ (km)	Window size (km × km)	Calculated bottom depth $z_b$ (km)			
			Conventional approach		Fractal approach	
			Centroid method	Spectral peak modeling (SPM)	Modified centroid method	Scaling-SPM
1	10	25 × 25	5.45	8	4	5.5
		50 × 50	13.1	11	8.38	8
		75 × 75	16.5	11.5	8.47	8.3
		100 × 100	18.7	12	10.1	11
		125 × 125	16.5	9	8.47	8.5
		150 × 150	20.0	10.5	12	9.4
		175 × 175	24.0	11	17.7	12.5
		200 × 200	26.4	13	15	12
		225 × 225	28	14	16	13.5
		250 × 250	29.5	18	15.7	13
2	18	25 × 25	5.93	5.5	5.23	6.5
		50 × 50	13.6	7.0	10.8	8
		75 × 75	20.6	14	12.6	15
		100 × 100	30.8	22	20.7	16.5
		125 × 125	41.3	25	24.3	20
		150 × 150	38.2	35	21.8	21
		175 × 175	42.0	37	23.9	21.5
		200 × 200	45.8	42	21.2	22
		225 × 225	38.6	42	21.4	20.5
		250 × 250	49.4	50	24.7	22
3	34	25 × 25	5.81	5.5	4.27	5.5
		50 × 50	10.9	8.0	12.2	7
		75 × 75	25.8	9.0	16.4	15
		100 × 100	39	13.0	23.9	19
		125 × 125	42.4	15.0	22.5	20
		150 × 150	39.3	18.0	23.8	22
		175 × 175	50.6	25.0	25.8	24
		200 × 200	57.7	38.0	26.5	20
		225 × 225	58.5	42.0	28.5	22
		250 × 250	66.5	45.0	32.9	25

$$P(k) = A_5 (e^{-|k|Z_t} - e^{-|k|Z_b})^2, \quad (8)$$

where  $A_5$  is a depth independent constant that can be used to shift the modeled spectra up and down to fit the spectral peak. A spectral peak is located in the lower range of wavenumbers of the spectra. The slope in the higher range of the wavenumbers is controlled by a combination of the depths to the top and bottom (Ravat et al., 2007). Equation (8) is rewritten for scaling distribution of sources,

$$P(k) = A_6 k^{-\beta} (e^{-|k|Z_t} - e^{-|k|Z_b})^2, \quad (9)$$

where  $A_6$  is constant. This method is called as scaling-SPM.

### 3. Synthetic Data

Two-dimensional synthetic magnetic fields are generated using the Pilkington and Todoeschuck (1993) approach, which is widely used in recent publications (e.g., Bouligand et al., 2009; Chen et al., 2016; Li et al., 2013). To produce a fractal 3-D magnetization volume, a three-dimensional magnetization model of dimension  $N \times N \times n$  of Gaussian noise is generated using  $1 \times 1 \times 1$  km cubic cells assigned with a mean magnetization of 100 A/m and standard deviation of 0.25 A/m, where  $N$  and  $n$  are the number of cells in horizontal and vertical dimensions, respectively. The 3-D random magnetization model is then Fourier

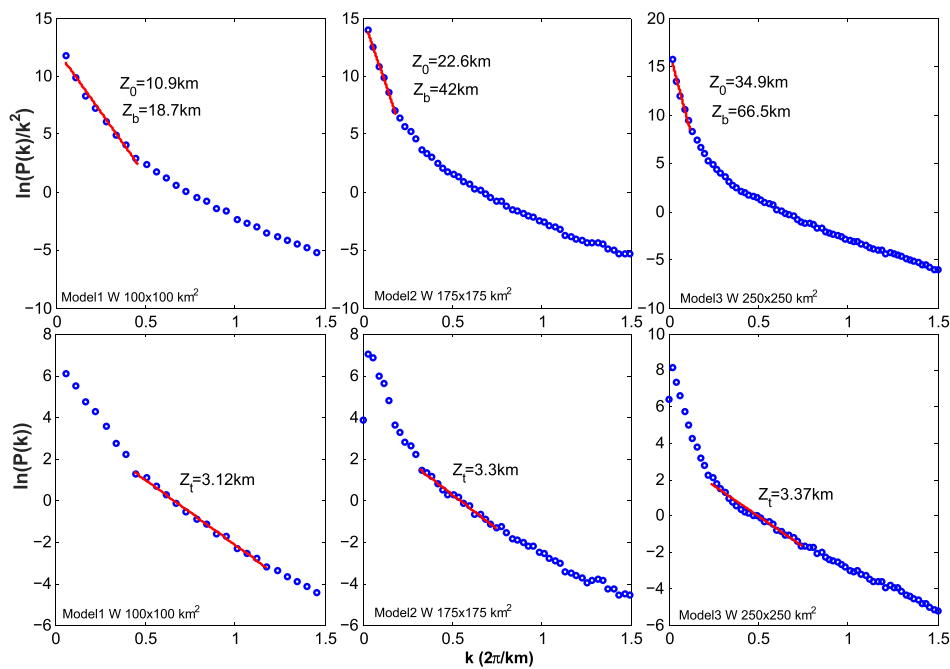


**Figure 2.** Plot of power spectrum vs. wavenumber for models 1, 2, and 3 with a window size of  $100 \times 100$ ,  $175 \times 175$ , and  $250 \times 250 \text{ km}^2$ , respectively. The depth to the top ( $Z_t$ ) (lower panel), centroid ( $Z_0$ ), and bottom ( $Z_b$ ) (upper panel) are estimated for each model using the centroid method. The radially averaged power spectrum is shown by blue circles and the red highlighted part of each curve shows the range of wavenumber used to estimate the depth. A constant depth of the top of 2 is assumed to produce all the models but depth of bottom for models 1, 2, and 3 are assumed to be 10, 18, and 34, respectively.

transformed and multiplied by  $(k_x^2 + k_y^2 + k_z^2)^{-\alpha/2}$  (Pilkington & Todoeschuck, 1993), where  $k_x$ ,  $k_y$ , and  $k_z$  are the wavenumbers in the  $x$ ,  $y$ , and  $z$  directions,  $\alpha$  is the scaling exponent of magnetization  $\alpha = \beta + 1$  (Maus & Dimri, 1994). Here we select  $\alpha = 3$  for 3-D sources as commonly used by many (e.g., Andrés et al., 2018; Bouligand et al., 2009; Fedi et al., 1997; Li et al., 2013, 2017). Subsequently, the modulated wavenumber domain model is inverse transformed into the space domain to obtain the fractal magnetization model. To calculate the magnetic anomaly of a given 3-D fractal magnetization model, we sum the magnetic anomaly at an elevation  $z$  above the slabs of the thickness of  $\Delta z$  extracted from the 3-D

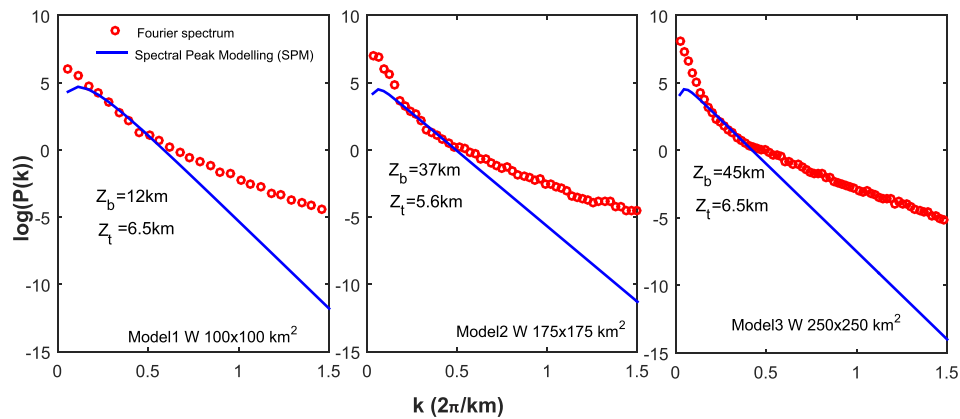


**Figure 3.** Estimation of DBMS using spectral peak modeling for models 1, 2, and 3 with a window size of  $100 \times 100$ ,  $175 \times 175$ , and  $250 \times 250 \text{ km}^2$ , respectively. The radially averaged power spectrum and the best fitted spectral peak modeling (SPM) curve are shown as red circles and solid blue lines, respectively.

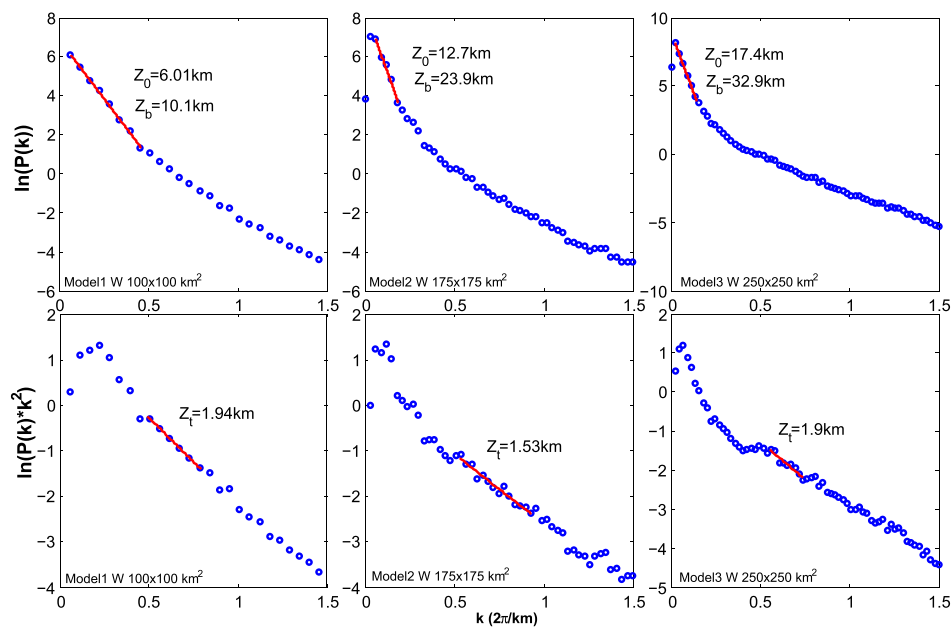


**Figure 4.** Plot of power spectrum vs. wavenumber for models 1, 2, and 3 with a window size of  $100 \times 100$ ,  $175 \times 175$ , and  $250 \times 250 \text{ km}^2$ , respectively. The depth to the top ( $Z_t$ ) (lower panel), centroid ( $Z_0$ ), and bottom ( $Z_b$ ) (upper panel) are estimated for each model using the modified centroid method.

magnetization volume. To calculate the magnetic anomaly of each slab, we multiplied the 2-D Fourier transform of the magnetization field of each of the slab by its corresponding Earth filter (Blakely, 1995). We generate magnetic anomalies for model 1, model 2, and model 3 using a constant depth to the top of 2 km and depths to the bottom of 10, 18, and 34 km, respectively. The 3-D magnetization model 3 ( $Z_t = 2 \text{ km}$ ,  $Z_b = 34 \text{ km}$ ) along with the magnetic anomalies of the three models are presented in Figure (1).

#### 4. Effect of Window Size in DBMS Estimation

The power spectra of different window sizes are computed for each synthetic case (Tables 1 and 2). Ten window sizes ranging from  $25 \times 25$  to  $250 \times 250 \text{ km}^2$  are used to study the effect of window size (Tables 1 and 2). In the centroid methods, we estimate the centroid and depths to the top of magnetic sources from lower and middle wavenumber ranges, respectively. Some of the authors estimated the depths by selecting

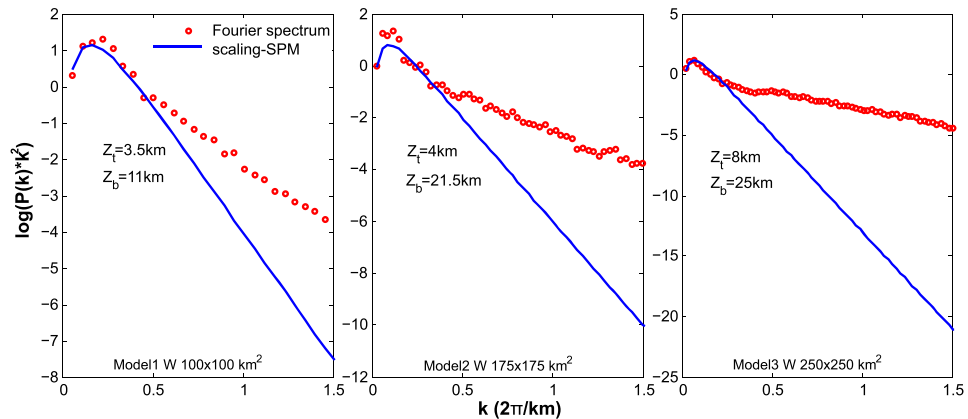


**Figure 5.** Estimation of DBMS using Scaling spectral peak modeling (scaling SPM) for models 1, 2, and 3 with a window size of  $100 \times 100$ ,  $175 \times 175$ , and  $250 \times 250 \text{ km}^2$ , respectively. The radially averaged power spectrum and the best fitted spectral peak modeling (SPM) curve are shown as red circles and solid blue lines, respectively.

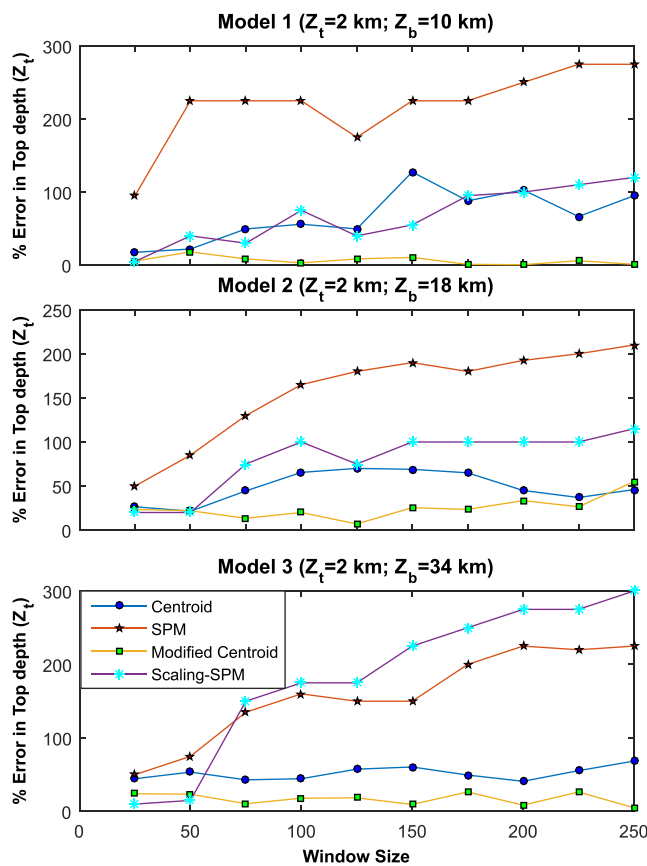


**Figure 6.** Percentage error in the depth to top estimation vs. window size for models 1, 2, and 3 using the centroid (blue circle), SPM (red star), modified centroid (green square), and scaling-SPM (cyan asterisk). The depth to the top has been assumed to be 2 km in all the three models.

are 2.89–3.37, 3.0–6.5, 1.52–1.90, and 1.8–8.0 km using the centroid method, SPM, modified centroid method, and scaling-SPM, respectively (Table 1). It is found that the centroid method estimates the depths to the top within 40–50% error whereas the errors in the modified centroid method estimates are below ~20% (Figure 6). The SPM methods and centroid method provide larger errors in the depth to the top estimations for all the window sizes once compared to the modified centroid method (Figure 6). We consider the modified centroid method as the most suited method for estimation of the depths to the top for all the models at all the window sizes within an error of 30%.

#### 4.2. Estimation of the DBMS

The DBMS and their errors are estimated using all the above-described methods and presented in Table 2 and Figure 7, respectively. For Model 1 ( $Z_t = 2$  km,  $Z_b = 10$  km), the DBMS for different window sizes are found to vary from 5.4–29.5, 8–18, 4.0–17.7, and 5.5–13.5 km using the centroid method, SPM, modified centroid method, and scaling-SPM, respectively (Table 2). The centroid method shows a large error (up to 200%) in the estimation of the DBMS (Figure 7). The SPM, modified centroid, and scaling-SPM methods provide an error estimation of  $\leq 40\%$  at window sizes of  $\geq 50 \times 50$  km<sup>2</sup>. The minimum error of ~5% is obtained at a window size of  $100 \times 100$  km from the modified centroid method (Figure 7).

For Model 2 ( $Z_t = 2$  km,  $Z_b = 18$  km), the estimated DBMS for different window sizes vary from 5.9–49.4, 5.5–50, 5.23–24.70, and 6.5–22.0 km using the centroid method, SPM, modified centroid method, and scaling-SPM, respectively (Table 2). The errors from scaling methods (modified centroid and scaling-SPM) are found within an error limit of ~20–30% for the window sizes of  $\geq 100 \times 100$  km (Figure 7). The conventional methods (centroid and SPM) provide smaller error, up to 30% for window sizes of  $\leq 100 \times 100$  km whereas larger

wavenumber range automatically irrespective of checking the slope in the spectra (e.g., Li et al., 2013, 2017). Some authors are in favor of selecting wavenumber range as per detectable slope for the respective window (e.g., Andrés et al., 2018; Bansal et al., 2011, 2013; Ravat et al., 2016). At the outset, we visually inspect for a clear linear feature in the plot within the range of lower and middle wavenumbers for each window. A straight line is fitted in the least square sense to these linear features and slopes are interpreted as depths to the top and bottom. In the SPM, we fit the spectral peak at low wavenumber range. The estimated DBMS for different window sizes using the centroid method, SPM, modified centroid, and scaling-SPM are presented in Figures 2–5, respectively. The percentage of errors of the top and bottom depths (DBMS) is computed as

$$\%error(depth) = abs\left(\frac{True\ depth - Estimated\ depth}{True\ depth}\right) \times 100. \quad (10)$$

#### 4.1. Estimation of the Depths to the Top of the Magnetic Sources

Model 1: The calculated ranges of the depths to the top for model 1 ( $Z_t = 2$ ,  $Z_b = 10$  km) using the centroid method, SPM, modified centroid method, and scaling-SPM are 2.4–4.6, 3.9–7.5, 1.6–2.2, and 1.9–4.4 km, respectively (Table 1). Error in the depths to the top increases significantly for larger window sizes regardless of the method used for its computation (Figure 6). The modified centroid method is found to provide smaller errors in the range of 5–10% for all the window sizes (Table 1).

For the second model ( $Z_t = 2$ ,  $Z_b = 18$  km), the depths to the top estimated between 2.43–3.40, 3.0–6.2, 1.53–3.10, and 1.6–4.0 km using the centroid method, SPM, modified centroid method, and scaling-SPM, respectively (Table 1). Similar to model 1, it is found that the modified centroid method gives smaller errors of up to ~30% when compared to the other three methods (Figure 6).

For the third model ( $Z_t = 2$ ,  $Z_b = 34$  km), the estimated depths to the top are 2.89–3.37, 3.0–6.5, 1.52–1.90, and 1.8–8.0 km using the centroid method, SPM, modified centroid method, and scaling-SPM, respectively (Table 1). It is found that the centroid method estimates the depths to the top within 40–50% error whereas the errors in the modified centroid method estimates are below ~20% (Figure 6). The SPM methods and centroid method provide larger errors in the depth to the top estimations for all the window sizes once compared to the modified centroid method (Figure 6). We consider the modified centroid method as the most suited method for estimation of the depths to the top for all the models at all the window sizes within an error of 30%.

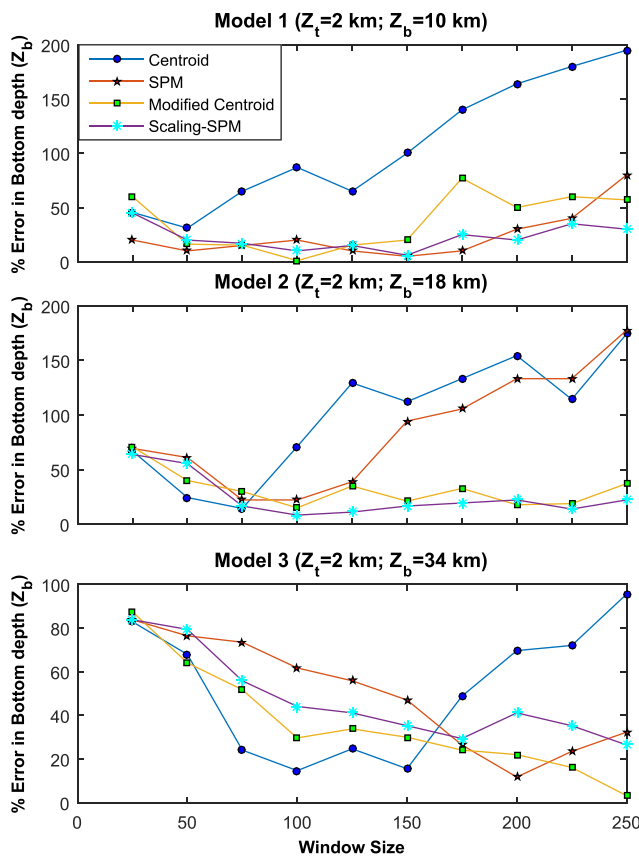


**Figure 7.** Percentage error in assumed bottom depth estimation vs. window size for model 1, model 2, and model 3, using the centroid method (blue circle), SPM (red star), modified centroid method (green square), and scaling-SPM (cyan asterisk). Models 1, 2, and 3 have the bottom depth of 10, 18, and 34 km, respectively.

error of the order of 70% is found for the larger window sizes ( $\geq 100 \times 100$  km). This error increases up to 150% for a window size of  $250 \times 250$  km. The earlier studies have shown that the conventional methods for uncorrelated distribution of sources provide an overestimation of the depth values (Bansal et al., 2016; Fedi et al., 1997; Maus & Dimri, 1994, 1995; Ravat et al., 2007).

For Model 3 ( $Z_t = 2$  km,  $Z_b = 24$  km), the calculated DBMS for different window sizes are found to vary from 5.8–66.5, 5.5–45.0, 4.3–32.9, and 5.5–25.0 km using the centroid method, SPM, modified centroid method, and scaling-SPM, respectively (Table 2). The errors are found to be ~20–30% for the window sizes  $> 150 \times 150$  km for the SPM, modified centroid method, and scaling-SPM whereas larger errors are found for smaller window sizes (Figure 7). The centroid method provides smaller errors for the window sizes  $< 150 \times 150$  km and larger errors, up to 90%, for the window sizes  $> 150 \times 150$  km (Figure 7).

The errors in the estimated DBMS are found ~20–30% for scaling distribution of sources (modified centroid and scaling-SPM) at window sizes  $\geq 50 \times 50$ ,  $\geq 100 \times 100$ ,  $\geq 150 \times 150$  km for the models 1, 2, and 3, respectively. The small errors are found for window sizes at least five times larger than the assumed DBMS. Therefore, a window size of  $\geq 5 \times$  targeted DBMS is the most suitable window size for the estimation of the DBMS. The SPM is providing an error of the order of 20–80% for models 1 and 3 at smaller window sizes. In the case of the SPM method, errors are ~20–30% at window sizes  $\leq 150 \times 150$  km for model 1 and  $< 20\%$  at window sizes of  $\geq 200 \times 200$  km for model 3 whereas larger errors are found for other window sizes. The error in the estimated DBMS values changes arbitrarily with window sizes. Therefore, we cannot establish an optimum window size for the SPM method. The conventional methods even provide good results for smaller window sizes mainly due to the nature of overestimation of the depths (Bansal et al., 2016; Blakely, 1995; Fedi et al., 1997; Spector & Grant, 1970).

## 5. Application to Iran Aeromagnetic Data

We apply the modified centroid method to the aeromagnetic data of Iran to calculate the DBMS values. Iran is made of different crustal blocks welded by a myriad of ophiolite belts and covered by voluminous Eocene volcanic belts and several large sedimentary basins (Figure 8). The complex geology of Iran provides an opportunity to test the applicability of the DBMS as a proxy for the estimation of Curie depth isotherm. Since the number of heat flow measurements in Iran is very sparse, we assess the applicability of the DBMS map in estimating the Curie depth by comparing our results against what is expected from tectonic of the study area, the Moho depth variations, and published Pn tomography maps.

During the last 300 Ma, the Iranian plateau has been forming on the southern border of the Laurasia supercontinent mostly by coalescing of several crustal pieces broken from the Gondwana supercontinent (e.g., Stampfli & Borel, 2002). The welding of different crustal pieces is supported by the presence of a wide network of ophiolite rocks (Figure 8). As part of the Alpine-Himalayan orogeny, the Iranian plateau is mostly the result of the collision of Arabian and Eurasian plates during Oligo-Miocene time (~32–25 Ma) (e.g., Agard et al., 2011). The plateau hosts different tectonic styles of collision and large-scale strike-slip faults (e.g., Hatzfeld & Molnar, 2010) (Figure 8). The collision has resulted in the formation of the Zagros, Alborz, Talesh, and Kopeh-Dagh mountain ranges, and the Sanandaj-Sirjan metamorphic zone (Figure 8). The presence of rigid blocks such as the South Caspian Basin and Lut (e.g., Jackson et al., 2002) further shaped the geometry and deformation of the orogenic belts. Northward subduction of the oceanic part of the Arabian plate beneath central Iran formed the Makran subduction zone in SE of Iran (e.g., McCall & Kidd, 1982). The subduction zone is composed of the world's largest subaerial accretionary prism, Jazmurian depression (i.e., possibly a fossil back-arc basin) (Shahabpour, 2010) and its associated volcanic arc.

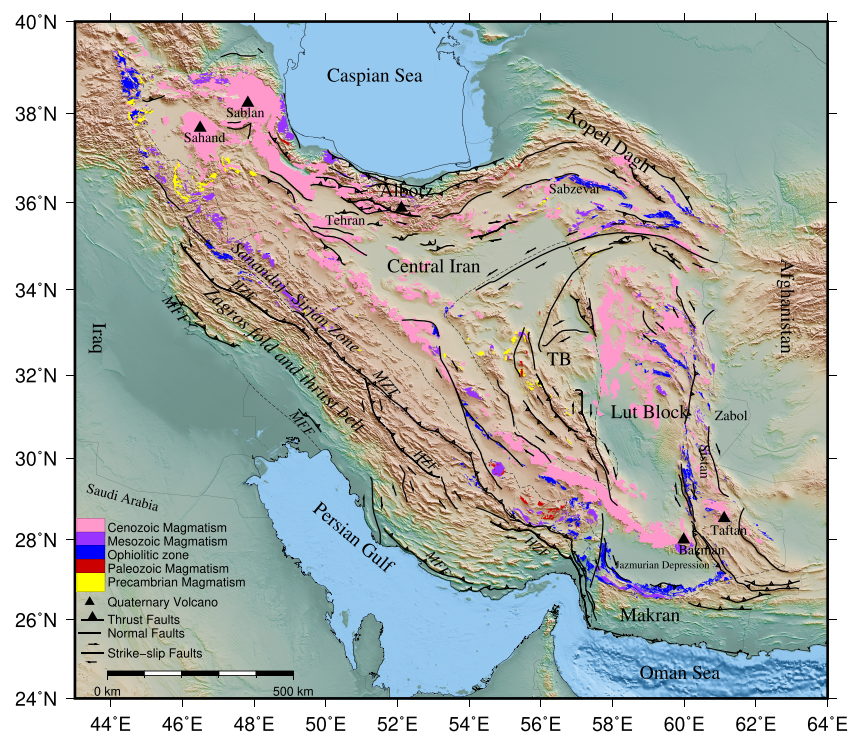


**Figure 8.** The geotectonic map of Iran showing the tectonic blocks. The active faults are presented by solid bold black lines with triangles and arrows. The abbreviations are TB = Tabas block; HZF = High Zagros Fault; MFF = Mountain Frontal Fault; MZT = Main Zagros Thrust.

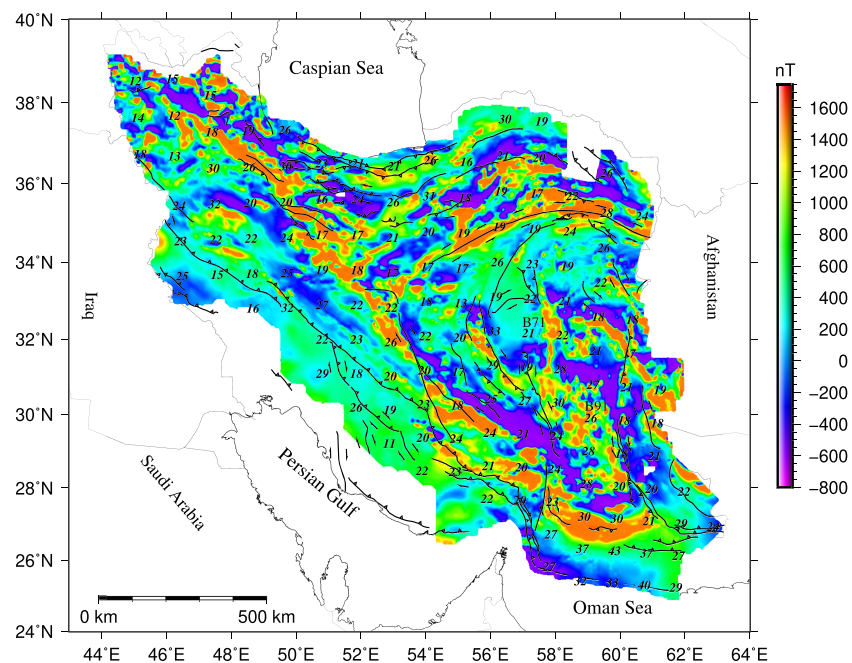


**Figure 9.** Aeromagnetic map of Iran. Numeric values at the center point of 200 × 200 km selected blocks, for radially averaged power spectrum, are estimated DBMS.

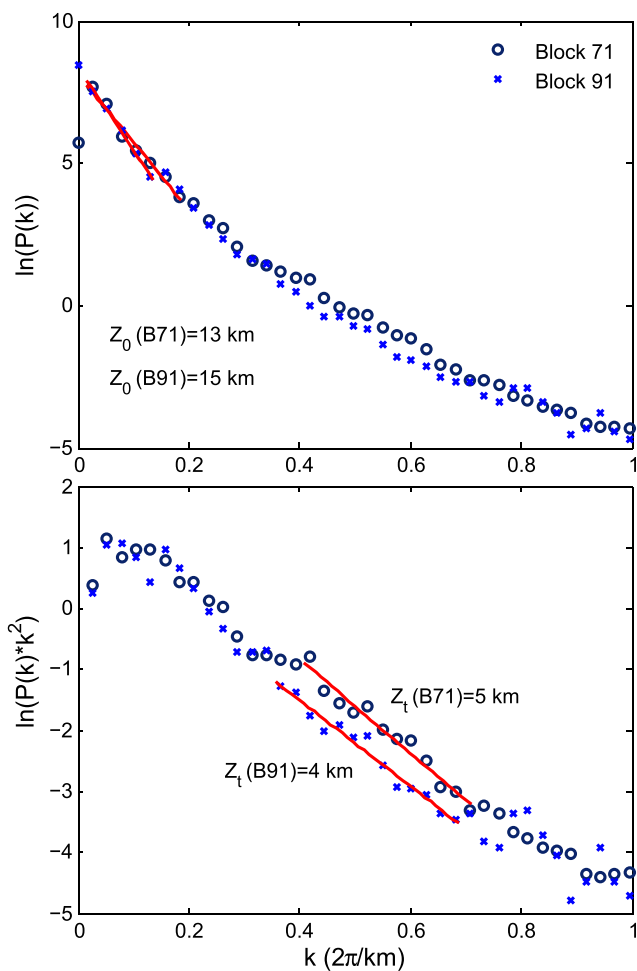


**Figure 10.** Power spectrum vs. wavenumber plot for blocks 71 and 91, the center location of the blocks is presented in Figure 9. The estimated centroid depths and depths to the top are shown individually.

of the 71 and 91 blocks (i.e., for the location of the center of the blocks see Figure 9) and present the estimated depth to the top and bottom of the magnetic layer for the blocks. The DBMS ranges in the main tectonic units of Iran are presented in Table 3.

The error estimation in the calculated DBMS is important to understand the reliability of its estimate. In statistical methods of regression analysis, the standard error in the slope is generally estimated (Crawley, 2007).

The depth to the top and centroid are half of the slope of the fitted straight line after applying the correction of scaling exponent in equations (4) and (6). The standard error,  $\epsilon$ , in the top and the centroid depths are computed separately as

$$\epsilon = \sqrt{\frac{1}{(n-2)} \left( \frac{\sum_{i=1}^n (P_i - \hat{P}_i)^2}{\sum_{i=1}^n (k_i - \bar{k})^2} \right)}, \quad (11)$$

where  $n$  is the number of observations,  $P_i$  and  $\hat{P}_i$  are the observed and estimated values of the corrected power spectrum,  $k_i$  and  $\bar{k}$  are observed and mean values of the wavenumber. The standard error in DBMS is calculated as,  $S_e = 2\epsilon_c + \epsilon_t$ , where  $\epsilon_c$  and  $\epsilon_t$  are the standard errors in the centroid and top depths, respectively.

**Table 3**  
*Estimated DBMS Range in the Main Tectonic Unit Over Iran*

Geological Unit	DBMS (km)
North-West Iran	12–18
Alborz	19–30
Kopeh Dagh	19–30
Central Iran	16–32
Tabas Block (TB)	13–33
Lut Block	17–30
Makran	24–43
Zabol	19
Sanandaj-Sirjan Zone	13–27
Zargos fold and thrust belt	11–32

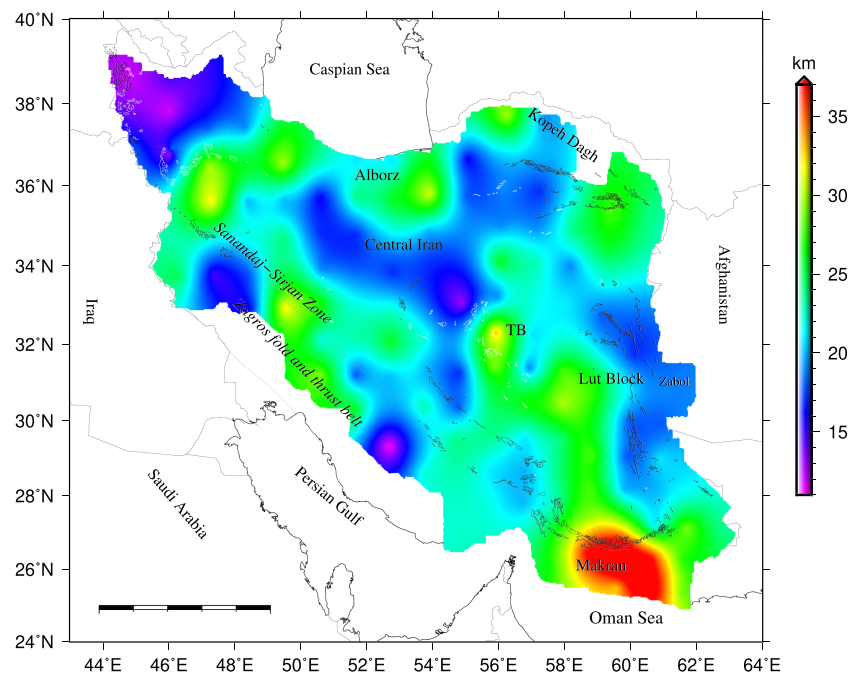


**Figure 11.** DBMS map of Iran. The estimated DBMS are ranging from 11 to 43 km. The black and white polygons are the Ophiolitic and Precambrian Magmatism, respectively.

## 6. Results and Discussion

Figure 11 shows the DBMS map of Iran. The most striking feature of the map is the deep DBMS (~40 km thick) over Makran accretionary wedge. The deep DBMS is in agreement with the presence of a thick sedimentary cover of >10 km (Teknik & Ghods, 2017) overlying over an old (~80–100 Ma, Gaina et al., 2015)

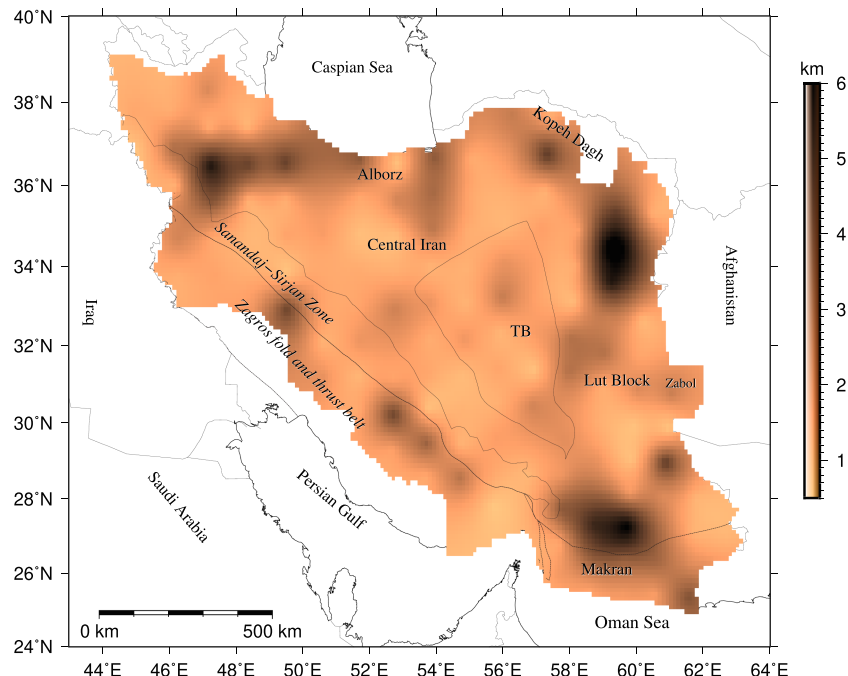


**Figure 12.** Map of standard error in the DBMS. The standard errors are varying from 0.5 to 6 km.

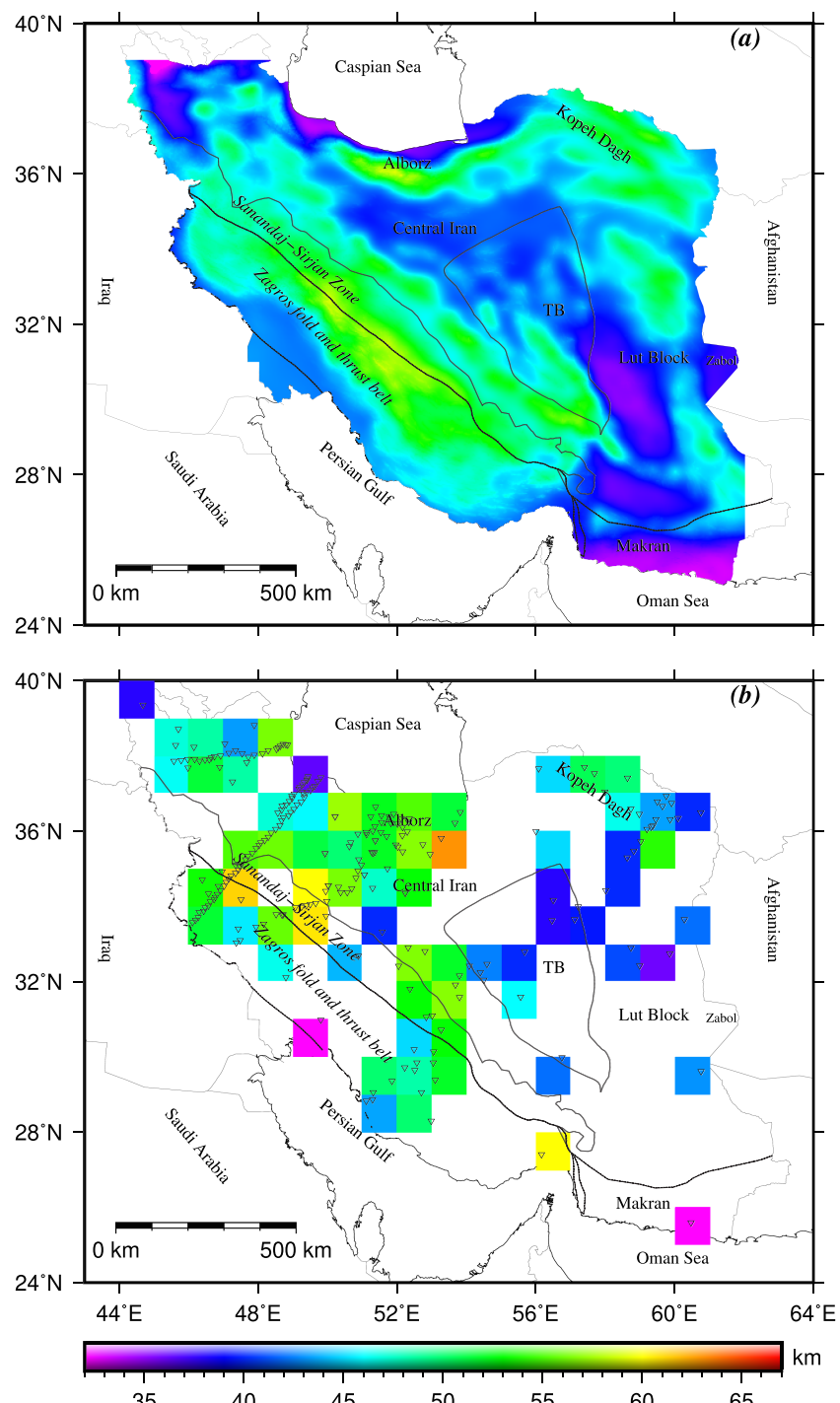


**Figure 13.** (a) The Moho map of Iran (after Jimenez-Munt et al., 2012) shows the large variations of crustal thickness in Iran ranging between 33 and 60 km. The crustal thickness in the Alborz mountains and the Zagros fold and thrust belt reach to about 55 km. (b) Moho map compiled from different studies (Sodoudi et al., 2009; Paul et al., 2010; Radjaee et al., 2010; Motaghi et al., 2015; Taghizade\_Farahmand et al., 2015; Teknik et al., 2019) based on receiver function analysis. Inverted triangles are the location of broadband seismic stations across Iran.

almost flat oceanic lithosphere (e.g., Penney et al., 2017). The oceanic plate cooling model of Stein and Stein (1992) suggests a depth of ~40 km for Curie isotherm of the oceanic lithosphere of age 80–100 Ma, closely in agreement with the calculated DBMS in the Makran accretionary wedge.

The DBMS of Iran (Figure 11) varies mostly in the range of 15–30 km excluding the deeper region in the Makran accretionary wedge whereas these values vary from 11 to 43 km. The standard errors in the DBMS varies from 0.5 to 6 km for the whole Iran (Figure 12). The DBMS may correspond to temperature or compositional boundary between magnetic and nonmagnetic lithosphere. The DBMS values are generally compared with the Moho depth to understand the magnetic behavior of the upper mantle. The Moho separates the crust from the upper mantle based on the seismic wave velocity discontinuity and reflects a compositional/mineralogical discontinuity. The behavior of the upper mantle depends on temperature, pressure, and mineral composition of the ultramafic rocks in the mantle (e.g., Ferre et al., 2014; Wasilewski et al., 1979; Wasilewski & Mayhew, 1992). The comparison of the DBMS (Figure 11) with the Moho depth (Figure 13) shows a weak correlation between the two maps and the DBMS is generally shallower than the Moho depth except in the Makran accretionary wedge.

Moho depth variations calculated by crustal gravity modeling (e.g., Jimenez-Munt et al., 2012; Figure 13a) and seismic receiver functions surveys (Sodoudi et al., 2009; Paul et al., 2010; Radjaee et al., 2010; Motagh et al., 2015; Taghizade\_Farahmand et al., 2015; Teknik et al., 2019; Figure 13b) show a significant crustal thickening beneath the Zagros Mountains. Since there is no volcanic activity within the Zagros mountain range (e.g., Agard et al., 2011), we expect a deeper Curie isotherm for the Zagros mountain range. Pn tomographic maps of Iran also support the presence of a cold upper mantle beneath the Zagros mountain range (Al-Lazki et al., 2004; Amini et al., 2012; Pei et al., 2011). Figure 11 shows that the DBMS mostly varies around 15–30 km over the Zagros but is overlain by two prominent shallow DBMS regions in NW Zagros and SE Zagros. The shallow DBMS regions encompass the two ophiolite outcrops along the Zagros suture zone (Figure 8). The shallow DBMS regions start around the Zagros suture zone and extend toward SW of Zagros, away from the main Zagros thrust fault, implying that the ophiolite emplacement extends over the Arabian plate. This finding shows that the DBMS is not a good proxy for Curie depth where ophiolite rocks are emplaced and instead it gives the depth to the bottom of the emplaced oceanic lithosphere. The DBMS does not necessarily coincide with Curie depth and it may be related to a change in lithology at depths shallower than the Curie depth. For example, the DBMS over the magnetized ophiolite rocks within Alp-Himalayan mountain ranges are expected to be shallower than Curie depth.

Like Zagros, many regions with shallow DBMS (such as regions along Sistan and Sabzevar suture zones) can be associated with the presence of ophiolite rocks. The only significant exception for the association of shallow DBMS regions with the outcrops of ophiolite rocks happens for the Makran subduction zone. Unlike other Ophiolites in Iran, the Makran Ophiolites are not a product of the continental collision and thus probably they do not significantly extend laterally with depth. Pn tomographic maps of Iran shows a relatively low-velocity zone for most of NW and Central Iran (Al-Lazki et al., 2004; Amini et al., 2012; Pei et al., 2011), predicting a relatively continuous region of DBMS. Figure 11 instead shows that Central Iran and NW Iran are composed of either relatively shallow or moderate DBMS values which again indicate a possibility of petrological variations instead of Curie depth variations.

There is a NE-SW trend of thick DMBS separating NW Iran from the rest of Central Iran. This is an interesting previously unknown trend that somehow is parallel to the NE-SW trend of the Precambrian basement in the region. The thicker DBMS trend is not related to the thickening of the crust along with the trend because no similar trend could be seen in the Bouguer gravity and crustal thickness maps (Dehghani & Makris, 1984; Jimenez-Munt et al., 2012; Figure 13a). The DBMS generally is significantly shallower to the north of the trend. The shallow DBMS is only partially related to the presence of ophiolite outcrops and probably partially related to the elevated geothermal gradients caused by two significant Quaternary Sabalan and Sahand volcanoes. A drastic change in the direction of the maximum stress axis happens across the trend, indirectly supporting the validity of the trend seen in our DBMS map. The direction of the maximum stress is N130 (Ghods et al., 2015) in the north of the trend whereas the direction of maximum stress in the south of the trend is N19E (Zarifi et al., 2014).

## 7. Conclusions

Estimation of the depth to the bottom of magnetic sources (DBMS) depends on the window size. The smaller the window size is the shallower the estimated depth. To ascertain the magnetic responses from the bottom of a magnetic layer, the optimum window size is required. The synthetic magnetic data are generated by

assuming three-dimensional fractal distribution of magnetization for three individual models of magnetic sources with the top ( $Z_t$ ) at 2 km and bottom ( $Z_b$ ) at 10, 18, 34 km, respectively. We calculated the error percentage for the depths to the top and DBMS for the window sizes of  $25 \times 25$ ,  $50 \times 50$ ,  $75 \times 75$ ,  $100 \times 100$ ,  $125 \times 125$ ,  $150 \times 150$ ,  $175 \times 175$ ,  $200 \times 200$ ,  $225 \times 225$ ,  $250 \times 250$  km<sup>2</sup>. The modified centroid method was found to be best suited for the estimation of the DBMS from the synthetic magnetic data. We applied the modified centroid method on aeromagnetic data of Iran for estimating DBMS. Across the Iranian plateau, the DBMS varies from 11 to 43 km but the dominant range is estimated between 15 and 30 km. The deepest DBMS of ~43 km corresponds to Makran accretionary wedge. The errors in DBMS estimation vary from 0.5 to 6 km. We found that the DBMS variations in Iran are very affected by the presence of ophiolites and thus can't be used as an efficient proxy for Curie isotherm.

### Acknowledgments

RK and ARB are thankful to Director, CSIR-NGRI, India for granting permission to publish this work. We thank V. P. Dimri, M. Pilkington, and G. Chen for useful discussion during this study. We are grateful to I. Jimenez-Munt and V. Teknik for providing the Moho map of Iran. We are grateful to Paul Tregoning, Editor, Bjarne Almqvist, associate editor, and two anonymous reviewers for useful comments on the manuscript. The aeromagnetic data used in the study are available at Zenodo.org (<http://doi.org/10.5281/zenodo.3554861>).

### References

- Agard, P., Omrani, J., Jolivet, L., Whitechurch, H., Vrielinck, B., Spakman, W., et al. (2011). Zagros orogeny: A subduction-dominated process. *Geological Magazine*, 148, 692–725. <https://doi.org/10.1017/S001675681100046X>
- Al-Lazki, A. I., Sandvol, E., Seber, D., Barazangi, M., Turkelli, N., & Mohamad, R. (2004). Pn tomographic imaging of mantle lid velocity and anisotropy at the junction of the Arabian, Eurasian and African plates. *Geophysical Journal International*, 158(3), 1024–1040. <https://doi.org/10.1111/j.1365-246X.2004.02355.x>
- Amini, S., Shomali, Z. H., Koyi, H., & Roberts, R. G. (2012). Tomographic upper-mantle velocity structure beneath the Iranian Plateau. *Tectonophysics*, 554–557, 42–49. <https://doi.org/10.1016/j.tecto.2012.06.009>
- Andrés, J., Marzán, I., Ayarza, P., Martí, D., Palomeras, I., Torné, M., et al. (2018). Curie point depth of the Iberian Peninsula and surrounding margins. A thermal and tectonic perspective of its evolution. *Journal of Geophysical Research: Solid Earth*, 123, 2049–2068. <https://doi.org/10.1002/2017JB014994>
- Bansal, A. R., Anand, S. P., Rajaram, M., Rao, V. K., & Dimri, V. P. (2013). Depth to the bottom of magnetic sources (DBMS) from aeromagnetic data of central India using modified centroid method for fractal distribution of sources. *Tectonophysics*, 603, 155–161. <https://doi.org/10.1016/j.tecto.2013.05.024>
- Bansal, A. R., & Dimri, V. P. (1999). Gravity evidence for mid crustal domal structure below Delhi fold belt and Bhilwara super group of western India. *Geophysical Research Letters*, 26, 2793–2795. <https://doi.org/10.1029/1999GL005359>
- Bansal, A. R., Dimri, V. P., Kumar, R., & Anand, S. P. (2016). Curie Depth estimation from aeromagnetic for fractal distribution of sources. In V. P. Dimri (Ed.), *Fractal solutions for understanding complex system in earth sciences*, (pp. 19–31). New York: Springer Earth System Sciences.
- Bansal, A. R., Gabriel, G., & Dimri, V. P. (2010). Power law distribution of susceptibility and density and its relation to seismic properties: An example from the German Continental Deep Drilling Program. *Journal of Applied Geophysics*, 72, 123–128. <https://doi.org/10.1016/j.jappgeo.2010.08.001>
- Bansal, A. R., Gabriel, G., Dimri, V. P., & Krawczyk, C. M. (2011). Estimation of the depth to the bottom of magnetic sources by a modified centroid method for fractal distribution of sources: An application to aeromagnetic data in Germany. *Geophysics*, 76, L11–L22. <https://doi.org/10.1190/1.3560017>
- Bhattacharyya, B. K., & Leu, L. K. (1975). Analysis of magnetic anomalies over Yellowstone National Park: Mapping of Curie point isothermal surface for geothermal reconnaissance. *Journal of Geophysical Research*, 80, 4461–4465. <https://doi.org/10.1029/JB080i032p04461>
- Bhattacharyya, B. K., & Leu, L. K. (1977). Spectral analysis of gravity and magnetic anomalies due to rectangular prismatic bodies. *Geophysics*, 42, 41–50. <https://doi.org/10.1190/1.1440712>
- Blakely, R. J. (1988). Curie temperature isotherm analysis and tectonic implications of aeromagnetic data from Nevada. *Journal of Geophysical Research*, 93, 11,817–11,832. <https://doi.org/10.1029/JB093iB10p11817>
- Blakely, R. J. (1995). *Potential theory in gravity & magnetic applications*. Cambridge: Cambridge University Press.
- Bouligand, C., Glen, J. M. G., & Blakely, R. J. (2009). Mapping Curie temperature depth in the western United States with a fractal model for crustal magnetization. *Journal of Geophysical Research*, 114, B11104. <https://doi.org/10.1029/2009JB006494>
- Chen, G., Cheng, Q., & Zhang, H. (2016). Matched filtering for separating magnetic anomaly using fractal model. *Computers and Geosciences*, 90, 179–188. <https://doi.org/10.1016/j.cageo.2016.02.015>
- Chiozzi, P., Matsushima, J., Okubo, Y., Pasquale, V., & Verdoya, M. (2005). Curie point depth from spectral analysis of magnetic data in central-southern Europe. *Physics of the Earth and Planetary Interiors*, 152, 267–276. <https://doi.org/10.1016/j.pepi.2005.04.005>
- Connard, G., Couch, R., & Gemperle, M. (1983). Analysis of aeromagnetic measurements from the Cascade Range in Central Orogen. *Geophysics*, 48, 376–390. <https://doi.org/10.1190/1.1441476>
- Crawley, M. J. (2007). *The R book*. Chichester: John Wiley & Sons Ltd. ISBN-13: 978-0-470-51024-7
- Dehghani, G., & Makris, J. (1984). The gravity field and crustal structure of Iran. *Geological Survey of Iran*, 51, 51–68. <https://doi.org/10.1127/njgpa/168/1984/215>
- Dimri, V. P. (2005). *Fractal behavior of the earth system*. New York: Springer.
- Dolmaz, M. N., Ustaomer, T., Hisarli, Z. M., & Orbay, N. (2005). Curie point depth variations to infer thermal structure of the crust at the African-Eurasian convergence zone, SW Turkey. *Earth, Planets and Space*, 57, 373–383.
- Fedi, M., Quarta, T., & Santis, A. D. (1997). Inherent power-law behavior of magnetic field power spectra from a Spector and Grant ensemble. *Geophysics*, 62, 1143–1150. <https://doi.org/10.1190/1.1444215>
- Ferre, E. C., Friedman, S. A., Hernandez, F. M., Feinberg, J. M., Till, J. L., Ionov, D. A., & Conder, J. A. (2014). Eight good reasons why the uppermost mantle could be magnetic. *Tectonophysics*, 624–625, 3–14. <https://doi.org/10.1016/j.tecto.2014.01.004>
- Gaina, C., Van Hinsbergen, D. J. J., & Spakman, W. (2015). Tectonic interactions between India and Arabia since the Jurassic reconstructed from marine geophysics, ophiolite geology, and seismic tomography. *Tectonics*, 34, 875–906. <https://doi.org/10.1002/2014TC003780>
- Ghods, A., Shabanian, E., Bergman, E., Faridi, M., Donner, S., Mortezanjad, G., & Aziz-Zanjani, A. (2015). The Varzaghān-Ahar, Iran, Earthquake Doublet (Mw 6.4, 6.2): Implications for the geodynamics of northwest Iran. *Geophysical Journal International*, 203, 522–540. <https://doi.org/10.1093/gji/gjv306>

- Hatzfeld, D., & Molnar, P. (2010). Comparisons of the kinematics and deep structures of the Zagros and Himalaya and of the Iranian and Tibetan plateaus and geodynamic implications. *Reviews of Geophysics*, 48, RG2005. <https://doi.org/10.1029/2009RG000304>
- Jackson, J., Priestley, K., & Berberian, M. (2002). Active tectonics of the South Caspian Basin. *Geophysical Journal International*, 148, 214–245. <https://doi.org/10.1046/j.1365-246X.2002.01588.x>
- Jimenez-Munt, I., Fernandez, M., Saura, E., Verges, J., & Garcia-Castellanos, D. (2012). 3-D lithospheric structure and regional/residual Bouguer anomalies in the Arabia-Eurasia collision (Iran). *Geophysical Journal International*, 190, 1311–1324. <https://doi.org/10.1111/j.1365-246X.2012.05580.x>
- Kumar, R., Bansal, A. R., Anand, S. P., Rao, V. K., & Singh, U. K. (2018). Mapping of magnetic basement in Central India from aeromagnetic data for scaling geology. *Geophysical Prospecting*, 66, 226–239. <https://doi.org/10.1111/1365-2478.12541>
- Li, C.-F., Lu, Y., & Wang, J. (2017). A global reference model of Curie-point depths based on EMAG2. *Nature Scientific Reports*, 7, 45129. <https://doi.org/10.1038/srep45129>
- Li, C.-F., Shi, X., Zhou, Z., Li, J., Geng, J., & Chen, B. (2010). Depths to the magnetic layer bottom in the South China Sea area and their tectonic implications. *Geophysical Journal International*, 182, 1229–1247. <https://doi.org/10.1111/j.1365-246X.2010.04702.x>
- Li, C.-F., Wang, J., Lin, J., & Wang, T. (2013). Thermal evolution of the north Atlantic lithosphere: New constraints from magnetic anomaly inversion with a fractal magnetization model. *Geochemistry, Geophysics, Geosystems*, 12, 5078–5105. <https://doi.org/10.1002/2013GC004896>
- Maus, S., & Dimri, V. P. (1994). Scaling properties of potential fields due to scaling sources. *Geophysical Research Letters*, 21, 891–894. <https://doi.org/10.1029/94GL00771>
- Maus, S., & Dimri, V. P. (1995). Potential field power spectrum inversion for scaling geology. *Journal of Geophysical Research*, 100, 12,605–12,616. <https://doi.org/10.1029/95JB00758>
- Maus, S., Gordon, D., & Fairhead, J. D. (1997). Curie temperature depth estimation using a self-similar magnetization model. *Geophysical Journal International*, 129, 163–168. <https://doi.org/10.1111/j.1365-246X.1997.tb00945.x>
- McCall, G. J. H., & Kidd, R. G. W. (1982). The Makran, Southeastern Iran: The anatomy of a convergent plate margin active from Cretaceous to Present. *Geological Society of London, Special Publication*, 10(1), 387–397. <https://doi.org/10.1144/GSL.SP.1982.010.01.26>
- Motagh, K., Tatar, M., Priestley, K., Romanelli, F., Doglioni, C., & Panza, G. F. (2015). The deep structure of the Iranian Plateau. *Gondwana Research*, 28, 407–418. <https://doi.org/10.1016/j.gr.2014.04.009>
- Okubo, Y., Graf, R. J., Hansen, R. O., Ogawa, K., & Tsu, H. (1985). Curie point depths of the island of Kyushu and surrounding area, Japan. *Geophysics*, 50, 481–489. <https://doi.org/10.1190/1.1441926>
- Okubo, Y., & Matsunaga, T. (1994). Curie point depth in northeast Japan and its correlation with regional thermal structure and seismicity. *Journal of Geophysical Research*, 99, 22,363–22,371. <https://doi.org/10.1029/94JB01336>
- Paul, A., Hatzfeld, D., Kaviani, A., Tatar, M., & Péquegnat, C. (2010). Seismic imaging of the lithospheric structure of the Zagros mountain belt (Iran). *Geological Society, London, Special Publications*, 330, 5–18. <https://doi.org/10.1144/SP330.2>
- Pei, S., Sun, Y., & Toksöz, M. N. (2011). Tomographic Pn and Sn velocity beneath the continental collision zone from Alps to Himalaya. *Journal of Geophysical Research*, 116, B10311. <https://doi.org/10.1029/2010JB007845>
- Penney, C., Tavakoli, F., Saadat, A., Nankali, H. R., Sedighi, M., Khorrami, F., et al. (2017). Megathrust and accretionary wedge properties and behaviour in the Makran subduction zone. *Geophysical Journal International*, 209, 1800–1830. <https://doi.org/10.1093/gji/ggx126>
- Pilkington, M., & Todoechuck, J. P. (1993). Fractal magnetization of continental crust. *Geophysical Research Letters*, 20, 627–630. <https://doi.org/10.1029/92GL03009>
- Pilkington, M., & Todoechuck, J. P. (1995). Scaling nature of crustal susceptibilities, *Geophysical Research Letters*, 22, 779–78. <https://doi.org/10.1029/95GL00486>
- Radjaei, A., Rham, D., Mokhtari, M., Tatar, M., Priestley, K., & Hatzfeld, D. (2010). Variation of Moho depth in the central part of the Alborz Mountains, northern Iran. *Geophysical Journal International*, 181, 173–184. <https://doi.org/10.1111/j.1365-246X.2010.04518.x>
- Ravat, D., Morgan, P., & Lowry, A. R. (2016). Geotherms from the temperature-depth constrained solutions of 1-D steady-state heat flow equation. *Geosphere*, 12, 1187–1197. <https://doi.org/10.1130/GES01235.1>
- Ravat, D., Pignatelli, A., Nicolosi, I., & Chiappini, M. (2007). A study of spectral methods of estimating the depth to the bottom of magnetic sources from near-surface magnetic anomaly data. *Geophysical Journal International*, 169, 421–434. <https://doi.org/10.1111/j.1365-246X.2007.03305.x>
- Ross, H. E., Blakely, R. J., & Zoback, M. D. (2006). Testing the use of aeromagnetic data for the determination of Curie depth in California. *Geophysics*, 71, L51–L59. <https://doi.org/10.1190/1.2335572>
- Saleh, R. (2006). Reprocessing of aeromagnetic map of Iran, M.Sc. Thesis supervised by A. Ghods, Institute for Advanced Studies in Basic Sciences, p169.
- Shahabpour, J. (2010). Tectonic implications of the geochemical data from the Makran igneous rocks in Iran. *Island Arc*, 19(4), 676–689. <https://doi.org/10.1111/j.1440-1738.2010.00723.x>
- Sodoudi, F., Yuan, X., Kind, R., Heit, B., & Sadikhouy, A. (2009). Evidence for a missing crustal root and a thin lithosphere beneath the Central Alborz by receiver function studies. *Geophysical Journal International*, 177, 733–742. <https://doi.org/10.1111/j.1365-246X.2009.04115.x>
- Spector, A., & Grant, F. S. (1970). Statistical model for interpreting aeromagnetic data. *Geophysics*, 35, 293–302. <https://doi.org/10.1190/1.1440092>
- Stampfli, G. M., & Borel, G. D. (2002). A plate tectonic model for the Paleozoic and Mesozoic constrained by dynamic plate boundaries and restored synthetic oceanic isochrones. *Earth and Planetary Science Letters*, 196, 17–33. [https://doi.org/10.1016/S0012-821X\(01\)00588-X](https://doi.org/10.1016/S0012-821X(01)00588-X)
- Stein, C. A., & Stein, S. (1992). A model for the global variation in oceanic depth and heat flow with lithospheric age. *Nature*, 359(6391), 123–129. <https://doi.org/10.1038/359123a0>
- Taghizade\_Farahmand, F., Afsari, N., & Sodoudi, F. (2015). Crustal thickness of Iran inferred from converted waves. *Pure and Applied Geophysics*, 172, 309–331. <https://doi.org/10.1007/s00024-014-0901-0>
- Tanaka, A., Okubo, Y., & Matsubayashi, O. (1999). Curie point depth based on spectrum analysis of the magnetic anomaly data in East and Southeast Asia. *Tectonophysics*, 306, 461–470. [https://doi.org/10.1016/S0040-1951\(99\)00072-4](https://doi.org/10.1016/S0040-1951(99)00072-4)
- Teknik, V., & Ghods, A. (2017). Depth of magnetic basement in Iran based on fractal spectral analysis of aeromagnetic data. *Geophysical Journal International*, 209, 1878–1891. <https://doi.org/10.1093/gji/gjx132>
- Teknik, V., Ghods, A., Thybo, H., & Artemieva, I. M. (2019). Crustal density structure of NW Iranian Plateau. *Canadian Journal of Earth Sciences*, 2(4), 1–61. <https://doi.org/10.1139/cjes-2018-0232>

- Wasilewski, P., & Mayhew, M. (1992). The Moho as magnetic boundary revisited. *Geophysical Research Letters*, 19, 2259–2262. <https://doi.org/10.1029/92GL01997>
- Wasilewski, P. J., Thomas, H. H., & Mayhew, M. A. (1979). The Moho as the magnetic boundary. *Geophysical Research Letters*, 6, 541–544. <https://doi.org/10.1029/GL006i007p00541>
- Zarifi, Z., Nilforoushan, F., & Raeesi, M. (2014). Crustal stress map of Iran: Insight from seismic and geodetic computations. *Pure and Applied Geophysics*, 171(7), 1219–1236. <https://doi.org/10.1007/s00024-013-0711-9>